

This is an Open Access document downloaded from ORCA, Cardiff University's institutional repository: <https://orca.cardiff.ac.uk/id/eprint/121629/>

This is the author's version of a work that was submitted to / accepted for publication.

Citation for final published version:

Dordevic, Luka, Marangoni, Tomas, Liu, Mingjie, De Zorzi, Rita, Geremia, Silvano, Minoia, Andrea, Lazzaroni, Roberto, Ishida, Yasuhiro and Bonifazi, Davide 2019. Templating porphyrin anisotropy via magnetically aligned carbon nanotubes. *ChemPlusChem* 84 (9) , pp. 1270-1278. 10.1002/cplu.201800623

Publishers page: <http://dx.doi.org/10.1002/cplu.201800623>

Please note:

Changes made as a result of publishing processes such as copy-editing, formatting and page numbers may not be reflected in this version. For the definitive version of this publication, please refer to the published source. You are advised to consult the publisher's version if you wish to cite this paper.

This version is being made available in accordance with publisher policies. See <http://orca.cf.ac.uk/policies.html> for usage policies. Copyright and moral rights for publications made available in ORCA are retained by the copyright holders.



# Templating porphyrin anisotropy via magnetically aligned carbon nanotubes

Luka Đorđević,<sup>a</sup> Tomas Marangoni,<sup>a</sup> Mingjie Liu,<sup>b</sup> Rita De Zorzi,<sup>a</sup> Silvano Geremia,<sup>a</sup> Andrea Minoia,<sup>c</sup> Roberto Lazzaroni,<sup>c</sup> Yasuhiro Ishida,<sup>b</sup> and Davide Bonifazi\*<sup>d</sup>

Dedication ((optional))

**Abstract:** We report the preparation and characterisation of a novel three-dimensional organic material consisting of porphyrin arrays on carbon nanotubes embedded in an organogel. Firstly, the porphyrin array was prepared through metal–ligand coordination of a ditopic ligand (1,2-bis(4-pyridyl)ethane) and two bis-Zn(II) porphyrins, linked through a pyrene core, and was studied through UV-Vis, NMR and diffusion spectroscopies. Secondly, the porphyrin supramolecular architecture was adsorbed on pristine carbon nanotubes, greatly improving the dispersibility of the latter in organic solvents. The hybrid material was characterised by means of UV-Vis, microscopic techniques and by thermogravimetric analysis. Finally, by exploiting the anisotropic magnetic susceptibility of carbon nanotubes, the hybrid material was aligned under a magnetic field, the organisation of which could be permanently kept by *in situ* gelation. The resultant hybrid organogel exhibited notable optical anisotropy, suggesting an anisotropic arrangement of the porphyrin-CNTs architectures in the macroscopic material.

## Introduction

Ordered and controlled nanostructures are one of the major routes towards new materials with outstanding properties. For example, just as Nature seamlessly arranges the light harvesting (LH) antenna complex in order to accomplish its unique functions,<sup>[1–3]</sup> chemists have devoted efforts in supramolecular association of fundamental molecular modules into functional materials.<sup>[4–13]</sup> In fact, the controlled organization of photoactive molecules is playing a crucial role in the research and future development of devices, such as solar cells,<sup>[14,15]</sup> organic transistors,<sup>[16,17]</sup> chemical and bio-sensors.<sup>[18–26]</sup> The organization into functional nano-architectures of chromophoric modules has been achieved either through non-templated or templated methodologies.<sup>[27]</sup> In case of non-templated approaches, the

various non-covalent interactions (*i.e.*, H-bonds, transition metal coordination bonds, electrostatic interactions and others) have been exploited to build complex organic architectures featuring nanoscale precision and long-range order.<sup>[28–31]</sup> The templated method, on the other hand, is based on exploiting interactions with substrates such as zeolites<sup>[32,33]</sup> and carbonaceous materials,<sup>[34–37]</sup> and has also been extremely useful in creating functional nanomaterials. Among the different chromophores, porphyrins, square planar tetrapyrrolic macrocycles comprising of 18π electrons, have arguably been the most exploited chromophores across different research disciplines.<sup>[38–45]</sup> Some of their advantageous properties include structural robustness, strong absorption properties in the UV-Vis spectral region and vast supramolecular chemistry.<sup>[46–53]</sup> Moreover, porphyrin chemistry has become extremely rich and diverse and the electronic and optical properties can be fine-tuned by shaping their periphery.<sup>[54–58]</sup> While a number of efforts in constructing nanostructures through the organization of porphyrins have been achieved, their organisation over multiple scales (from the nanoscale to the microscale) remains of great interest owing to their potentials in light-harvesting applications.<sup>[59–63]</sup> Although one- or two-dimensional supramolecular porphyrin systems are now easily prepared, the construction of three-dimensional assemblies remains a challenge.<sup>[64–66]</sup> While porphyrin low-dimensional oligomers have already been prepared, both by the templated<sup>[67–</sup>

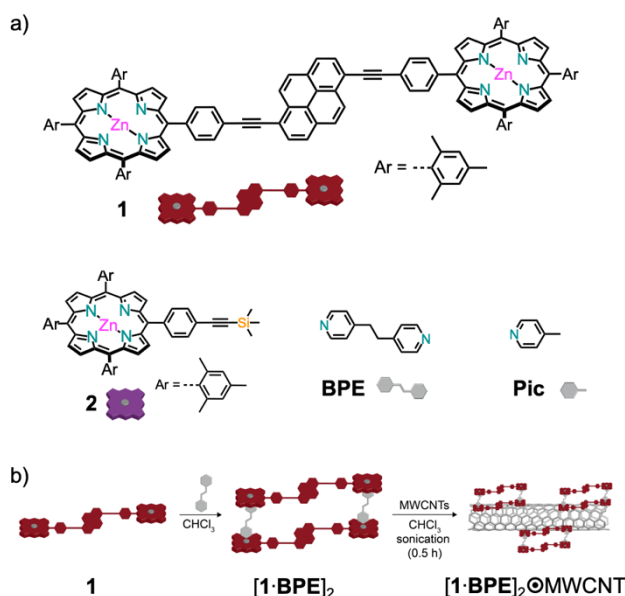


**Figure 1.** (a) Compounds 1, 2, Picoline (Pic) and 1,2-bis(4-pyridyl)ethane (BPE) used in this study and (b) preparation of the [1·BPE]<sub>2</sub> and the subsequent dispersion of MWCNTs.

[a] Dr. L. Đorđević, Dr. T. Marangoni, Dr. R. De Zorzi, Prof. S. Geremia  
Department of Chemical and Pharmaceutical Sciences, University of Trieste

Via L. Giorgieri 1, 34127 Trieste, Italy

[b] Dr. M. Liu and Prof. Y. Ishida  
RIKEN Center for Emergent Matter Science  
2-1 Hirosawa, Wako, Saitama 351-0198, Japan

[c] Dr. A. Minoia and Prof. R. Lazzaroni  
Laboratory for Chemistry of Novel Materials, CIRMAP, Université de Mons-UMONS

Place du Parc 20, B-7000 Mons, Belgium

[d] Prof. D. Bonifazi  
School of Chemistry, Cardiff University  
Park Place Main Building, CF10 3AT. E-mail:  
bonifazi@d@cardiff.ac.uk

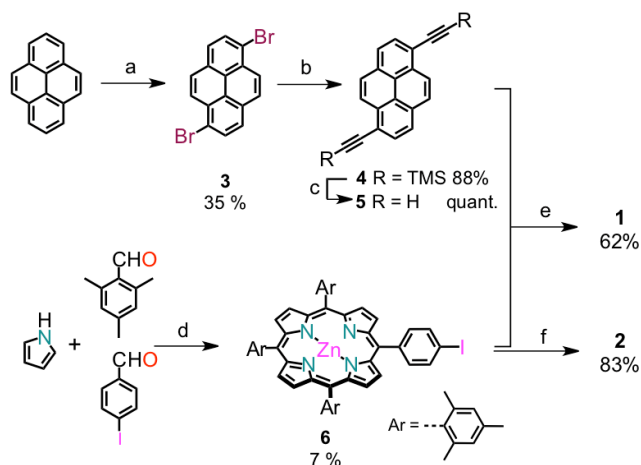
Supporting information for this article is given via a link at the end of the document.

71] and non-templated approaches,<sup>[72,73]</sup> we strived to

macroscopically arrange porphyrin structures through magnetically aligned multi-walled carbon-nanotubes (MWCNTs).<sup>[74–77]</sup> CNTs appear to be the ideal platform due to their versatility in interacting with organic molecules, such as porphyrins,<sup>[78–83]</sup> OPEs,<sup>[84–87]</sup> TTFs,<sup>[88,89]</sup> perylene bisimides,<sup>[90,91]</sup> alkylated fullerenes<sup>[92–95]</sup> and various supramolecular architectures.<sup>[96–103]</sup> The supramolecular porphyrin array used in this study was prepared by preparing a 1:1 mixture of bis-tetrapyrrolic macrocycle **1** and the ditopic ligand 1,2-bis(4-pyridyl)ethane (**BPE**), through metal-ligand complexation (N⋯Zn), in a CHCl<sub>3</sub> solution (Figure 1). Compound **1** was designed to bear a central pyrene unit, which could act as anchoring moiety to form known pyrene-CNTs π-π interactions that, in turn, can aid with the dispersion of CNTs.<sup>[104–108]</sup> This hybrid material [**1**·**BPE**]<sub>2</sub>⊂MWCNT resulted in a very stable suspension that could be aligned under a magnetic field. Aiming at preserving the alignment after the stimulus was removed, hybrid [**1**·**BPE**]<sub>2</sub>⊂MWCNT was mixed with poly(hydroxybutyrate-co-hydroxyvalerate) (PHBV, 4 mol % PHV content), an organic biodegradable polymer that is known to form organogels.<sup>[109]</sup>

## Results and Discussion

**Syntheses.** The synthetic pathway undertaken to obtain compounds **1** and **2** is reported in Scheme 1. Compound **1** is comprised of a central aromatic core, 1,6-disubstituted pyrene, and two peripheral Zn(II)-porphyrin units. Moreover, the Zn(II)-porphyrin bears three mesityl units around its core in order to avoid additional π-π interactions with the MWCNTs and self-aggregation (Figure S1, Supporting Information). The two synthons were prepared following literature procedures<sup>[110–112]</sup> and were connected exploiting a Pd(0)-catalysed Cu-free



**Scheme 1.** Synthetic route to obtain compounds **1** and **2**: (a) Br<sub>2</sub>, CCl<sub>4</sub>, rt; (b) TMSA, [Pd(PPh<sub>3</sub>)<sub>2</sub>Cl<sub>2</sub>], PPh<sub>3</sub>, CuI, THF/Tol/Et<sub>3</sub>N, 120 °C, 1 h, μW irradiation; (c) K<sub>2</sub>CO<sub>3</sub>, CHCl<sub>3</sub>/MeOH, rt; (d) **1**. BF<sub>3</sub>·Et<sub>2</sub>O, CHCl<sub>3</sub>, 1 h, rt; **2**. DDQ, 1 h, rt; **3**. Et<sub>3</sub>N, 15 min, rt; **4**. Zn(OAc)<sub>2</sub>·2H<sub>2</sub>O, CHCl<sub>3</sub>/MeOH; (e) [Pd<sub>2</sub>(dba)<sub>3</sub>], AsPh<sub>3</sub>, Tol/Et<sub>3</sub>N, rt; (f) TMSA, [Pd<sub>2</sub>(dba)<sub>3</sub>], AsPh<sub>3</sub>, Tol/Et<sub>3</sub>N, rt. Abbreviations: TMSA, trimethylsilylacetylene; THF, tetrahydrofuran; Tol, toluene; DDQ, 2,3-dichloro-5,6-dicyanobenzoquinone.



**Figure 2.** X-ray structure of compound **1**. With two methanol molecules coordinated to the Zn centres. Hydrogens atoms are omitted for clarity. Color coding: C (gray), N (purple), O (red).

Sonogashira cross-coupling reaction<sup>[113]</sup> in 62% yield. Suitable crystals for X-ray crystallography were grown by vapour diffusion of MeOH into a CHCl<sub>3</sub> solution of **1**, with the structure being shown in Figure 2. Monotopic porphyrin **2** was analogously prepared, through Pd(0)-catalysed cross-coupling reaction, between porphyrin **6** and trimethylsilylacetylene in 83% yield.

**Porphyrin Array Formation.** First of all, we set to study the formation of the porphyrin array [**1**·**BPE**]<sub>2</sub> in a CHCl<sub>3</sub> solution. While the coordination chemistry of Zn(II) porphyrins has been studied in detail,<sup>[46,114]</sup> we first investigated the influence of mesityl peripheral groups on the metal coordination (N⋯Zn). In order to appreciate the impact of the substituted phenyl groups on the axial coordination, we performed UV-Vis titration ( $c = 3.0 \times 10^{-6}$  M, CHCl<sub>3</sub>, 298 K) of porphyrin **2** with 4-picoline (**Pic**) (Figure 3a and S2, Supporting Information). The progressive addition of **Pic** into a solution of **2**, resulted in a bathochromic shift of the Soret band from 421 to 431 nm. Non-linear global regression analysis,<sup>[115]</sup> gave a microscopic binding constant  $K_m = 1.8 \times 10^4$  M<sup>-1</sup>. This is in great agreement with the value obtained by <sup>1</sup>H-NMR titration for the same system ( $K_m = 1.6 \times 10^4$  M<sup>-1</sup>, Figure S3, Supporting Information). Subsequently, we performed UV-Vis titration ( $c = 1.8 \times 10^{-5}$  M, CHCl<sub>3</sub>, 298 K) experiments to prove the interaction between compound **1** and **BPE** (Figure 3b). A bathochromic shift of the Q bands was observed (from 550 and 590 nm to 565 and 605 nm, respectively), thus confirming the N⋯Zn coordination.

To gain further insights into the structural changes upon binding of the ligand to compound **1**, <sup>1</sup>H-NMR of a 1:1 mixture ( $c = 1.1 \times 10^{-3}$  M, CHCl<sub>3</sub>, 298 K) was performed (Figure 3c). The clearest change upon addition of one equivalent (eq.) of **BPE** is the appearance of three additional peaks at 5.05, 3.05 and 1.25 ppm, attributed to the bis-pyridyl protons that show a significant upfield shift (compared to the free **BPE**). Changes were also observed in the chemical shift and multiplicity of the porphyrin protons, namely an upfield shift for all β-pyrrolic signals of around 0.15 ppm was observed. These observations prompted us to perform <sup>1</sup>H-NMR titrations ( $c = 1.1 \times 10^{-3}$  M, CHCl<sub>3</sub>, 298 K, Figures 3d and S4, Supporting Information) to elucidate the dynamic and structural evolution occurring upon the binding of the ligand. The addition from zero to one eq. of **BPE** showed the upfield shift of the α, β and -(CH<sub>2</sub>)<sub>2</sub>- signals of the ditopic pyridine ligand at 5.05, 3.05 and 1.25 ppm. Addition of more than one eq. of ligand showed the progressive downfield shift of the ligand signals toward those of the free species, indicating a fast equilibrium. More useful structural information was obtained by observing the evolution of the β-pyrrolic signals upon addition of the ligand. From zero to one eq. of **BPE**, the β-pyrrolic protons showed a progressive upfield shift and an increased multiplicity due to the diminished symmetry

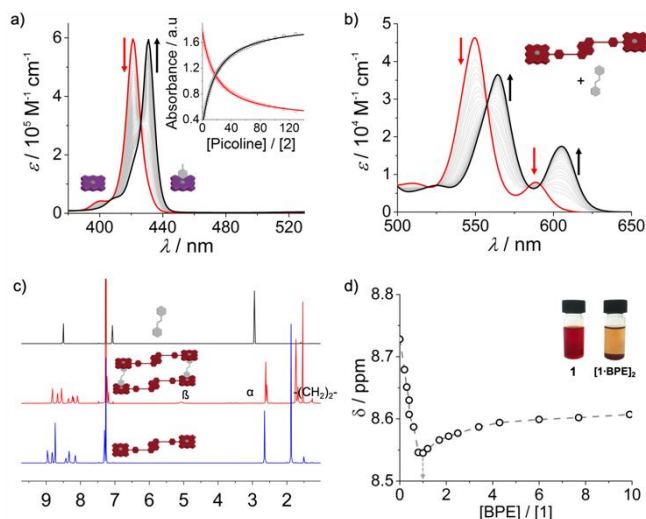


**Figure 3.** Selected spectroscopic investigations: (a) UV-Vis titration data ( $\text{CHCl}_3$ , 298K) of compound **2** ( $c = 3.0 \times 10^{-6}$  M) with different molar amounts of **Pic** (from 0 to 150 equivalents); inset shows the variation in absorbance at 421 nm (red circles) and 431 nm (black circles) plotted against the molar ratio with the corresponding 1:1 non-linear least-square fitting; (b) UV-Vis titration data ( $\text{CHCl}_3$ , 298 K) of compound **1** ( $c = 1.8 \times 10^{-5}$  M) with different molar amounts of **BPE** (from 0 to 36 equivalents); (c)  $^1\text{H-NMR}$  ( $\text{CDCl}_3$ , 298 K,  $c = 1.1 \times 10^{-3}$  M) of **BPE** (top), compound **1** (bottom) and their 1:1 mixture (middle),  $\alpha$ ,  $\beta$  and  $-(\text{CH}_2)_2-$  indicate the signals of complexed **BPE**; (d)  $^1\text{H-NMR}$  ( $\text{CDCl}_3$ , 298K) titration of compound **1** ( $c = 1.1 \times 10^{-3}$  M) with **BPE**, experimental data for  $\beta$ -pyrrole protons ppm shift against **BPE** eq.; the grey dotted line is intended as guide for the eye; inset shows a  $1.1 \times 10^{-3}$  M solution of **1** before (left) and after (12 h, right) titration experiment.

of compound **1** upon coordination. Addition of more than one eq. of the ligand maintained the increased multiplicity of the  $\beta$ -pyrrolic signals, but a downfield shift was observed. The experimental data in Figure 3d are diagnostic of a closed 2:2 sandwich that progressively moves toward the  $[\mathbf{1} \cdot (\text{BPE})_2]$  complex.<sup>[116,117]</sup> Unfortunately, the precipitation of the complex, which occurs upon progressive addition of ligand to the solution (Figure 3d inset, Figure S4, Supporting Information, note the baseline changes even if  $n$  scans remains constant) made it impossible to obtain a precise fit. To further characterise the structure of the coordination complex, Diffusion-Order Spectroscopy (DOSY) measurements of solutions containing the single components or the 1:1 mixture were performed (Figure 4). This powerful technique has become the method of choice for multi-component systems in order to gain the structural insights of their effective size and shape.<sup>[118,119]</sup> In this context, diffusion NMR spectroscopy would help us to determine the species in solution, even if some precipitate is formed. The self-diffusion translational coefficient ( $D_f$ ) of the species showed a slight decrease of the  $D_{exp}$  of a 1:1 mixture, when compared to compound **1** alone (Figures 4b,c). This observation alone would exclude the formation of oligomeric/polymeric species in solution. Additional analysis of the DOSY data allowed us to compare the  $D_f$  with the respective molecular weights ( $MW$ ). For rod-like species, such as those considered here, the ratio of the diffusion coefficients for two different molecular species ( $D_1/D_2$ ) is inversely proportional to the square root of the ratio of their molecular weights ( $M_2/M_1$ ):  $D_1/D_2$

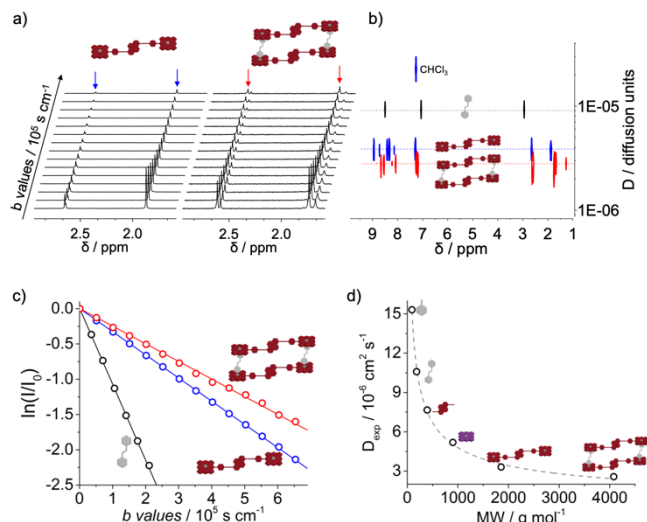


**Figure 4.** DOSY investigation (a) stack plot showing the signal decays as a function of gradient strength ( $G$ ) for compounds **1** and  $[\mathbf{1} \cdot (\text{BPE})_2]$ ; (b) overlay of three 2D-DOSY experiments – **BPE** (black), compound **1** (blue) and  $[\mathbf{1} \cdot (\text{BPE})_2]$  (red); (c) normalised signal decays ( $\ln(I/I_0)$ ) versus the diffusion weighing ( $b$  values) of representative peaks of **BPE** (black), **1** (blue) and  $[\mathbf{1} \cdot (\text{BPE})_2]$  (red) with the corresponding linear fits; (d) graphical analysis of  $D_{exp}$  values for different molecules used in this study; the dotted lines represent the calculated correlation of diffusion coefficients and molecular weights assuming that the diffusion coefficients for two different molecular species ( $D_1/D_2$ ) is inversely proportional to the square root of the ratio of their molecular weights  $M_2/M_1$  for rod-like species.

$= (M_2/M_1)^{1/2}$ .<sup>[120,121]</sup> Thus, by comparing these ratios (Table 1 and Figure 4d) we could confirm the formation of  $[\mathbf{1} \cdot (\text{BPE})_2]$  in solution.

**Table 1.** Diffusion coefficients ( $D_{exp}$ ) determined by DOSY experiments. Molecular weights ( $MW$ ) and the relation between diffusion coefficients and molecular weights (compared to **BPE**) for rod-like species are reported. Complete information is found in Supporting Information (Figures S5-7 and Table S1).

Sample	Diff. Coeff. ( $\times 10^{-6} / \text{cm}^2 \text{ s}^{-1}$ )	$MW$ (g/mol)	$D_{BPE} / D_h$	$(MW_n / MW_{BPE})^{1/2}$
<b>BPE</b>	10.59	184.24	1.00	1.00
<b>1</b>	3.31	1854.94	0.31	0.32
$[\mathbf{1} \cdot (\text{BPE})_2]$	2.57	4078.36	0.24	0.21

**Dispersion of MWCNTs.** Adapting a recently reported procedure for the non-covalent functionalization of CNTs with organic molecules,<sup>[99]</sup> it was possible to functionalise and disperse MWCNTs with  $[\mathbf{1} \cdot (\text{BPE})_2]$  (Figure 5), by means of multiple cycles of dispersion/centrifugation steps. Samples of  $[\mathbf{1} \cdot (\text{BPE})_2] \odot \text{MWCNT}$  were prepared by sonication (rt, 30 min) of 1.0 mg of pristine MWCNTs into a 1:1 molar ratio solution of **1** and **BPE** in  $\text{CHCl}_3$  ( $c = 4.9 \times 10^{-5}$  M). The resulting black suspension was then centrifuged (at 5 krpm) for 30 min in order to separate the unfunctionalised and aggregated fraction of carbonaceous material from the dispersed nanotubes. Finally, the supernatant solution was separated, filtered, and washed with  $\text{CHCl}_3$  to

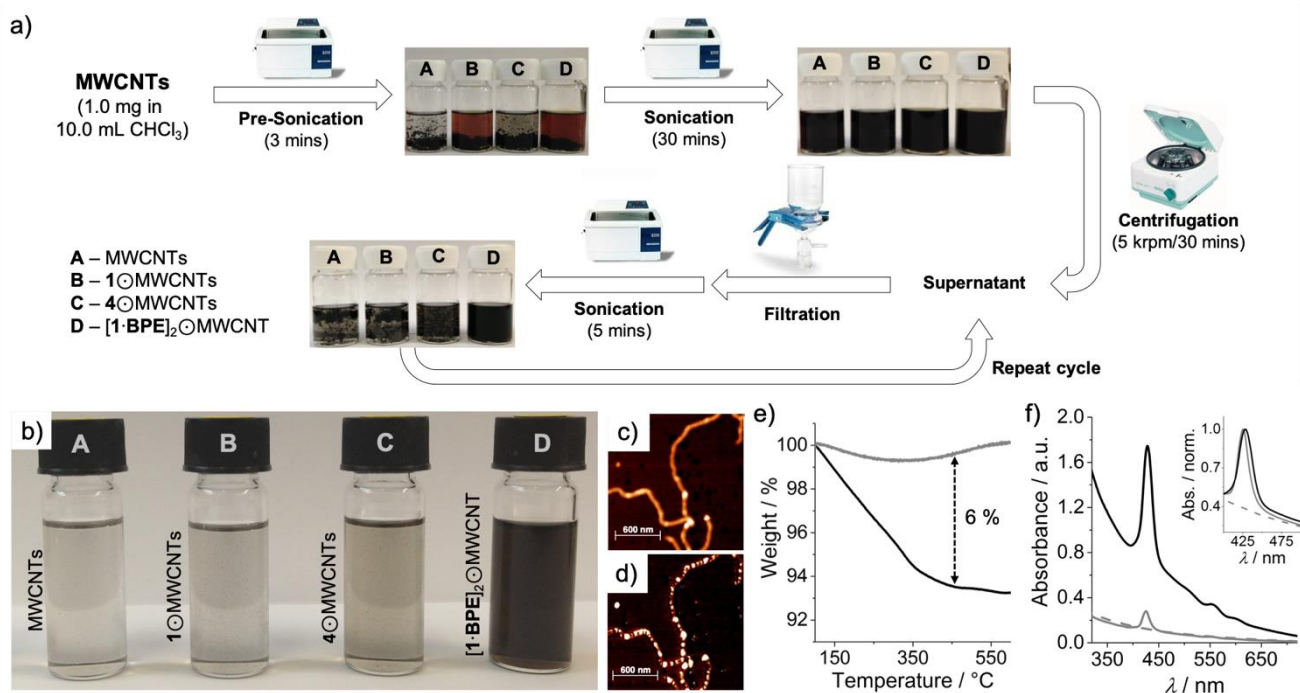


**Figure 5.** (a) Protocol adopted for the non-covalent dispersion of CNTs: to a suspension of MWCNTs in CHCl<sub>3</sub> (1.0 mg in 10.0 mL) was pre-sonicated and organic material was added ( $c = 4.9 \times 10^{-5}$  M). This suspension was sonicated for 30 minutes, centrifuged for 30 minutes, then the dispersed nanotubes were taken from the supernatant and this solution was filtered to remove the excess organic material. The solid was redispersed in 10.0 mL CHCl<sub>3</sub> and sonicated for 5 minutes to obtain a stable suspension. This process was repeated until UV-Vis absorption showed no excess organic material in the filtrate; (b) enlarged photograph of the dispersions obtained from the non-covalent dispersion protocol; (c,d) topography and phase TM-AFM images of the [1-BPE]<sub>2</sub>@MWCNT; (e) thermogravimetric analysis of the [1-BPE]<sub>2</sub>@MWCNT (black line) in comparison to the pristine MWCNTs (grey line) showing a weight loss of 6% at 450 °C; (f) UV-Vis spectra of the [1-BPE]<sub>2</sub>@MWCNT (black), 1@MWCNT (grey) and 4@MWCNT (dashed), the inset shows the normalised absorption of the 3 hybrids.

remove the excess of the organic material. Multiple cycles were performed until the filtrate showed no UV-Vis absorption profiles. The same procedure was used in order to determine whether other compounds used in this study could disperse the MWCNTs. With compounds **1**, **2** and **4** only traces (< 5%) of the hybrid material were detected; in contrast, complex [1-BPE]<sub>2</sub> gave a high dispersibility of the carbon nanomaterial. The dispersibility was also confirmed by means of tapping mode atomic force microscopy (TM-AFM). Indeed, a drop-casted solution of [1-BPE]<sub>2</sub>@MWCNT showed only the presence of individualised CNT structures (Figures 5c,d), indicating the efficient de-bundling action triggered by [1-BPE]<sub>2</sub>. A closer analysis of the [1-BPE]<sub>2</sub>@MWCNT material clearly showed the presence of tubular structures having lumps along the nanotubes (Figure 4d), which were not present in the case of the pristine MWCNTs (Figure S11, Supporting Information). These periodic structures can be possibly attributed to the sandwiched [1-BPE]<sub>2</sub> complexes, which are adsorbed around the MWCNTs thus enhancing their dispersibility. Furthermore, the presence of soft organic material onto the CNT surface was observed by phase imaging of [1-BPE]<sub>2</sub>@MWCNT (Figure 5d). Indeed, phase analysis revealed the presence of areas of the sample possessing different contrast which could be ascribed to the adsorption of organic material possessing different viscoelastic properties than that of the graphitic CNTs.

The presence of the organic compound on the nanotubes was also investigated by recording the UV-Vis absorption and emission profiles. The UV-Vis spectra of [1-BPE]<sub>2</sub>@MWCNT showed the characteristic absorption profiles of dispersed nanotubes, along with the typical electronic Soret and Q transitions originating from the porphyrin macrocycle (Figures 5f and S9, Supporting Information). Fluorescence spectroscopy (Figure S10, Supporting Information) showed a weak emission profile suggesting that, as expected, was strongly quenched upon adsorption on the nanotube framework. Final evidence of the formation of the hybrid material was obtained through thermogravimetric analysis (TGA). At 450 °C the hybrid material presents a 6% loss in weight when compared to the pristine MWCNTs (Figure 5e), with the weight loss attributed to the presence of the organic material. Finally, we proved that the functionalisation of the MWCNTs<sup>[99,100,122]</sup> is reversible (Figure S11, Supporting Information) by employing a strong acid (trifluoroacetic acid, TFA, capable of protonating both the porphyrin and the ligand) or by heating.

**Molecular Modelling.** Molecular modelling simulations have been performed in order to gain some understanding on the morphology of the [1-BPE]<sub>2</sub>/CNT interface in the [1-BPE]<sub>2</sub>@MWCNT hybrid material (Figure 6). The Biovia molecular modelling package Materials Studio 7 has been used to perform such modelling,<sup>[123]</sup> using its implementation of the

COMPASS force field.<sup>[124]</sup> Only the outermost tube of the MWCNTs has been considered for the modelling, assuming that the main contribution to the stability of the  $[1\cdot\text{BPE}]_2\text{MWCNT}$  interface is coming from the adsorption on the MWCNTs external wall, which we represent as an infinite, rigid carbon nanotube having a diameter of about 10 nm. The first step in building the

molecular model for the  $[1\cdot\text{BPE}]_2/\text{CNT}$  interface was to compare the interaction between the nanotube wall and compound **1** when adsorbed in flat and edge-on geometries. The  $1\text{MWCNT}$  interaction energy,  $E(1\text{MWCNT})$ , is calculated as the sum of the electrostatic and dispersion (vdW) energies between compound **1** and the nanotube and the results show that compound **1** is

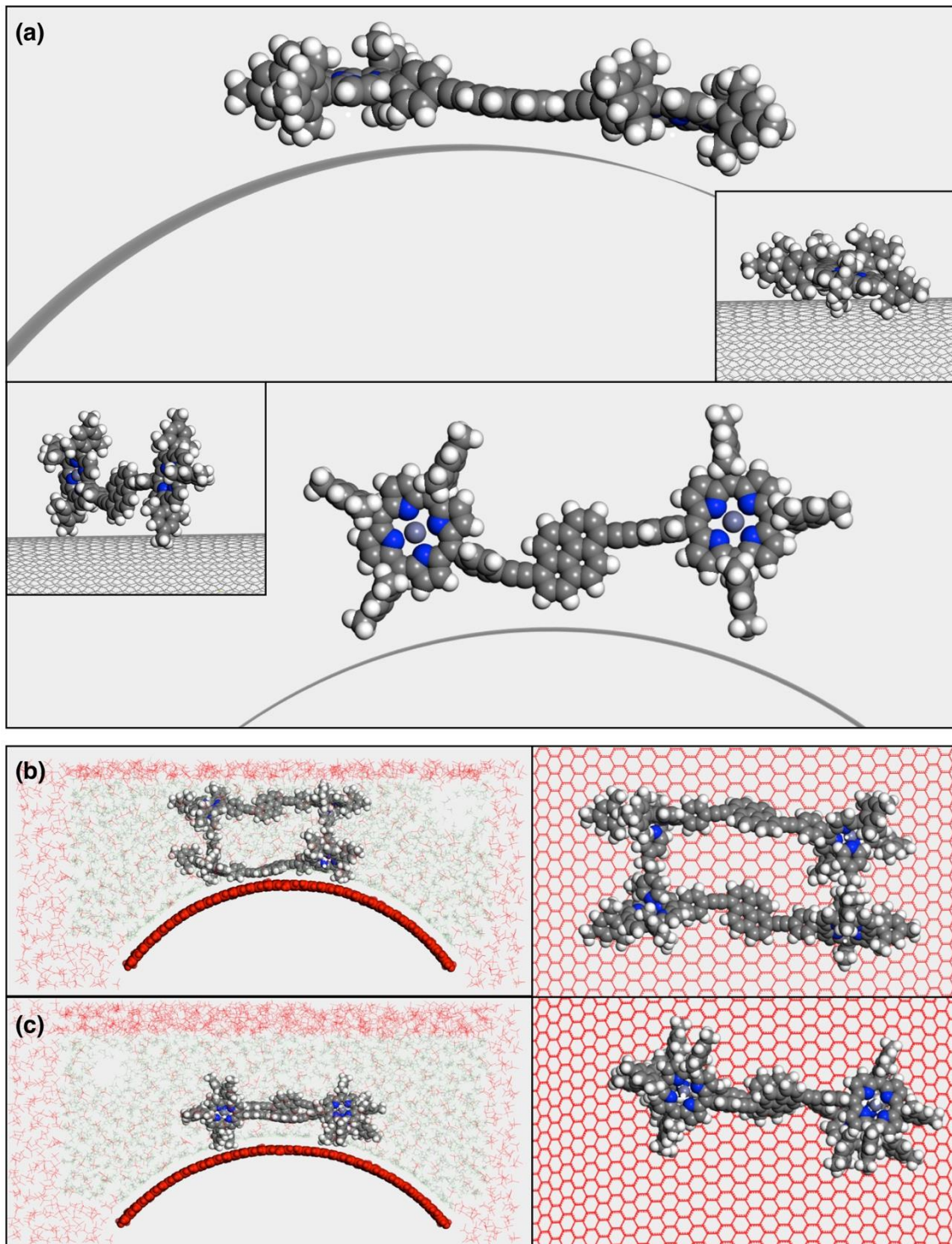


**Figure 6.** (a) Front and side view of compound **1** adsorbed flat (top) and edge-on (bottom) on the nanotube; (b) most stable conformations for  $[1\cdot\text{BPE}]_2\text{MWCNT}$  complex adsorbed flat and (c) edge-on on the nanotube; Figures b,c left show the full system where the fixed molecules are shown in red. Figures b,c right show the top views of the adsorbed geometries.

about 67 kcal mol<sup>-1</sup> more stable when adsorbed flat on the nanotube (Figure 6a top) than when it is adsorbed in an edge-on orientation (Figure 6a bottom). This is due to the fact that when compound **1** is adsorbed flat, (i) favourable  $\pi$ - $\pi$  interactions can be formed between its pyrene fragment and the nanotube wall, and (ii) less torsional stress is present in its molecular structure. The much higher stability of the flat orientation is also reflected in the observation that when initially set in the edge-on orientation, compound **1** will spontaneously go flat on the nanotube in just a few ps of MD simulation. Next, we built the [1·BPE]<sub>2</sub> complex and made it interact with the surface of the nanotube in a bath of CHCl<sub>3</sub>. The adsorption on the CNT surface of the [1·BPE]<sub>2</sub> complex was investigated during 100-ps long molecular dynamic simulations, both in the flat (Figure 6b left) and edge-on (Figure 6c left) geometries. Finally, an iterative MD/Quench scheme<sup>[125]</sup> consisting in a series of short (20-ps) MD, followed by a geometry optimization of the system, is used to obtain the most stable conformations of the [1·BPE]<sub>2</sub> complex in the flat and edge-on geometries (Figure 6b,c right). The stability of the interfaces is then estimated by comparing the [1·BPE]<sub>2</sub>⊙MWCNT interaction energies, and the results show that the interface where the [1·BPE]<sub>2</sub> complex is adsorbed flat on the nanotube is about 42 kcal mol<sup>-1</sup> more stable than that where the complex is adsorbed edge-on. This difference can be rationalised considering the complete adsorption of one porphyrin unit on the nanotube, whereas in the edge-on geometry the only interactions between the complex and the carbon surface are present through some methyl groups on the mesityl arms. These results indicate that the [1·BPE]<sub>2</sub> complex prefers to interact with the nanotube by having one porphyrin fully adsorbed on the surface and the other one solvated.

**Magnetic alignment.** At this point, the CNTs, through their magnetic susceptibility,<sup>[126]</sup> could be used for the templated alignment of the adsorbed organic material as a top-down approach.<sup>[127–131]</sup> However, the alignment can hold only when a magnetic field is applied, thus using only a solution of hybrid material would be unpractical. To this end, we used an organic biodegradable polymer (poly(hydroxybutyrate-co-hydroxyvalerate, PHBV, with a PHV content 4 mol %) that, in the presence of organic solvent, would swell and gel relatively fast (Figure 7). By employing different amounts of organogel, one can tune the gelation time, the optical transparencies and the manifestation of the magnetic behaviour.<sup>[132]</sup> The best results were obtained for 10.0 mg of 4% PHBV and applying the magnetic field for 60 minutes. The optimised procedure for the formation of the aligned hybrid material is depicted in Figure 7a: to 10.0 mg solid was added a solution of hybrid [1·BPE]<sub>2</sub>⊙MWCNT (1.0 mL) and the mixture was briefly heated to solubilise the organogel. At this point, toluene (2.0 mL) was added to the heated solution and the solution (final concentration of 3.3 mg mL<sup>-1</sup>) was placed under a magnetic field (*B*, 10 T) and left until gelation was complete. Considering the direction of the magnetic field, one could imagine a “side-wall” face of the hybrid gel is parallel to *B* and a “tip” perpendicular to *B*. The first evidence of anisotropic absorption was observed with the polarised optical microscope (POM) under a crossed Nicols (Figure 7c). The microscope displayed very

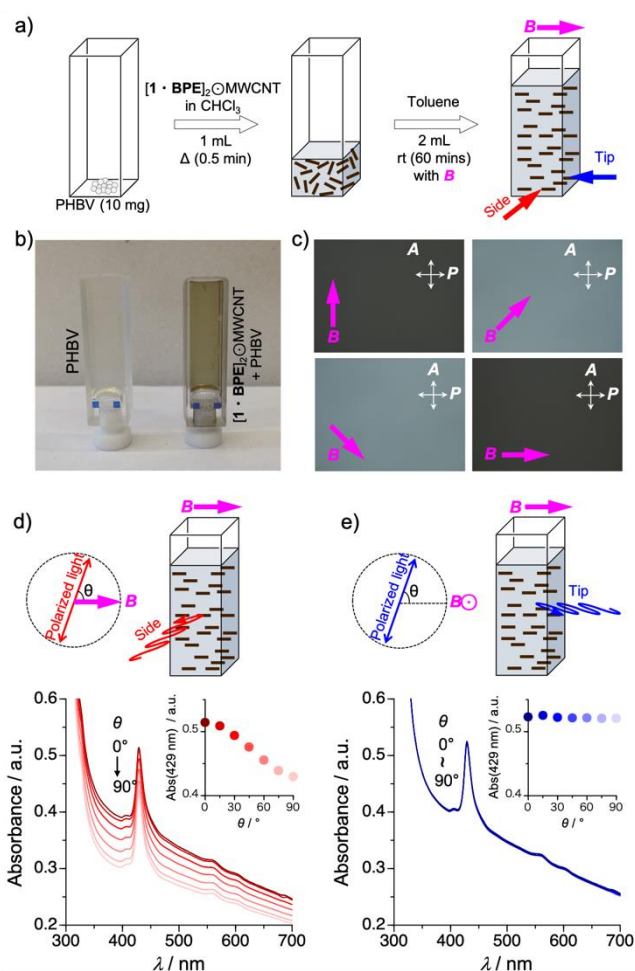


**Figure 7.** (a) Steps adopted in the preparation of the aligned hybrid organogel containing [1·BPE]<sub>2</sub>⊙MWCNT; (b) photograph of the PHBV-alone organogel (left) and aligned hybrid organogel (right); (c) POM images of the “side-wall” face of the aligned hybrid organogel; (d,e) UV-Vis absorption profiles recorded at different polarised angles ( $\theta =$  from 0°  $\rightarrow$  90° by 15° steps) of the “side-wall” face (d) and the “tip” face (e).

different image brightness depending on the rotation of the sample. When the “side-wall” face of the aligned hybrid organogel was rotated in an in-plane manner, its POM showed a contrast every 45°, giving a dark image when the light polarization angle with respect the applied magnetic field was either 0° or 90°. When performing measurements on the “tip” edge of the aligned hybrid organogel no difference in brightness was perceived (Figure S12, Supporting Information). In order to assess whether the goal of building a three-dimensional templated porphyrin hybrid was successful, we performed polarised UV-Vis absorption spectroscopy (Figure 7d,e). When rotating the “side-wall” face and measuring the absorption spectra every  $\theta = 15^\circ$  (Figure 7d), a stepwise reduction in the overall absorbance (including the Soret and Q-bands, centred at 429 and 553 nm) was observed from  $\theta = 0^\circ$  (maximum absorbance) to  $\theta = 90^\circ$  (minimum absorbance). This further proved the alignment of the porphyrin organisation exerted by the CNT template. Additional

experiments at the “tip” face (Figure 7e) showed an optical isotropic behaviour, namely no changes in the absorption intensity were detected at different incident angles ( $\theta =$  from  $0^\circ \rightarrow 90^\circ$  by  $15^\circ$  steps). In parallel, reference materials, containing either PHBV alone or PHBV with only the  $[1\text{-BPE}]_2$  complex were also prepared to pinpoint the templating effect of the CNT framework. Isotropic optical behaviour was obtained when performing UV-Vis absorption measurements on both the PHBV-alone organogel and the hybrid material containing only chromophore  $[1\text{-BPE}]_2$  (in both cases with a polymer concentration at  $3.3 \text{ mg mL}^{-1}$ , Figure S13, Supporting Information), thus further confirming the templating efficacy exercised by the tubular carbon framework.

## Conclusions

We report the development of a novel hybrid material comprising a chromophore array adsorbed on carbon nanotubes and embedded in an organogel. The chromophores are made of a supramolecular porphyrin array built by metal-ligand coordination and was thoroughly characterized in solution before being adsorbed on carbon nanotubes. The hybrid material was then characterized, and molecular modelling used in order to gain insight in the interaction. Finally, magnetic manipulation of the hybrid material, and the subsequent locking of the orientation in an organogel, showed optical anisotropy, suggesting anisotropic arrangement of the porphyrin arrays due to the templating effect of the carbon nanotubes. This paves the way for new applications of these functional materials since the information, partitioned by the magnetic field on the templated chromophore, could be preserved over time. Such hybrid materials could be used to fabricate field-effect transistors,<sup>[133]</sup> solar cells<sup>[134]</sup> and tailoring charge-transfer processes.<sup>[135]</sup> Further efforts could be also directed in preparing anisotropic hydrogels and exploiting the mechanical toughness, actuating and electroconductive properties.<sup>[131]</sup>

## Experimental Section

**Materials and Methods.** Melting points are uncorrected.  $^1\text{H}$  and  $^{13}\text{C}$  NMR spectra were measured using a *Varian* Inova spectrometer at 500 and 125 MHz, respectively. Chemical shifts are reported in parts per million (ppm) and are referenced to the residual solvent peak. Coupling constants ( $J$ ) are given in hertz (Hz). The Self-diffusion coefficient evaluations were carried out using *Varian* Inova (500 MHz) NMR spectrometer equipped with Performa II-Z gradient coils with a *cc\_BPPSTE* pulse sequence. Microwave irradiation was performed using CEM Discovery Reactor, using a dynamic mode of 200 W maximum power. UV-Vis spectra were recorded on a *Varian* Cary 5000 spectrometer. Fluorescence spectra were recorded with a *Varian* Cary Eclipse spectrophotometer. IR spectra (KBr) were recorded on a Perkin Elmer 2000 spectrometer. (HR)-MALDI-MS mass spectrometry was performed by the Centre de spectrométrie de masse at the Université de Mons in Belgium recorded using a Waters QToF

Premier mass spectrometer. Teflon(JH)Millipore® ( $0.45 \mu\text{m}$ ) filters were used in order to recover functionalised carbon nanotubes from a chloroform solution. Tapping-mode AFM measurements were carried out in air at 293 K by using a Nanoscope IIIa (Digital Instruments Metrology Group, USA) instrument, model MMAFMLN. Sonication was performed using a Branson 2510 Ultrasonic Bath. TGA analyses were performed using a TA Instruments TGA Q500 with a ramp of  $10^\circ\text{C}/\text{min}$  under  $\text{N}_2$  from 100 to  $800^\circ\text{C}$ . Magnetic alignment was performed on a superconducting magnet JASTEC 10T100 with a vertical bore of 100 mm was used for magneto-induced orientation of MWCNTs. Polarised optical microscopy (POM) was performed on a Nikon model Eclipse LV100POL optical polarizing microscope. Polarised UV-Vis spectra were recorded on a JASCO V-670 UV/Vis/NIR spectrophotometer.

Chemicals were purchased from Aldrich, Fluka, and Acros and used as received. Solvents were purchased from JT Baker, Aldrich and VWR, and deuterated solvents from Aldrich and Cambridge Isotope Laboratories. Thin layer chromatography (TLC) was conducted on pre-coated aluminium sheets with  $0.20 \text{ mm}$  *Machevery-Nagel* Alugram SIL G/UV254 with fluorescent indicator UV<sub>254</sub>. Column chromatography was carried out using Merck Gerduran silica gel 60 (particle size  $15\text{-}40$  and  $40\text{-}63 \mu\text{m}$ ). MWCNTs are Nanocyl 7000, batch 318-25. Characterization spectra of compound **1** are in the Supporting Information (Figures S14-S18). CCDC 1432475 (**1**) contains the supplementary crystallographic data for this paper - these data can be obtained free of charge from The Cambridge Crystallographic Data Centre.

### Syntheses.

#### 1,6-Bis-[(Zn(II)-5-(1-phen-4-yl)-10,15,20-

trimesitylporphyrin)ethynyl]pyrene (**1**): To a Schlenk tube, a solution of  $\text{Zn(II)-5-(4-iodophenyl)-10,15,20-}$ trimesitylporphyrin<sup>[110]</sup> (50.0 mg,  $53.7 \mu\text{mol}$ ) in toluene/ $\text{Et}_3\text{N}$  (5:1, 15.0 mL) was added and the whole was degassed with a freeze-pump-thaw cycle. After this,  $[\text{Pd}(\text{dba})_3]$  (12.3 mg,  $13.4 \mu\text{mol}$ ) and  $\text{AsPh}_3$  (16.4 mg,  $53.6 \mu\text{mol}$ ) were added and the suspension was subjected to another degassing cycle. Finally, 1,6-diethynylpyrene **5**<sup>[111]</sup> (5.0 mg,  $24.4 \mu\text{mol}$ ) was added and all was degassed for the last time. All was stirred at room temperature overnight, under argon atmosphere. The reaction mixture was filtered over celite (with the aid of  $\text{CH}_2\text{Cl}_2$ ), evaporated, purified by column chromatography ( $\text{CHX}/\text{CH}_2\text{Cl}_2$ , 85:15 v/v) and further purified by precipitation from  $\text{CH}_2\text{Cl}_2$  with cold petroleum ether to obtain the pure product as dark red solid (62% yield, 28.0 mg). Crystals suitable for X-ray were obtained from  $\text{CHCl}_3/\text{MeOH}$ . m.p.  $> 300^\circ\text{C}$ .  $^1\text{H-NMR}$  (500 MHz,  $\text{CDCl}_3$ ):  $\delta$  8.97-8.93 (m, 6 H, Ar-*H* +  $\beta$ -pyrrole), 8.82 (d,  $J = 4.6$ , 4 H,  $\beta$ -pyrrole), 8.74 (s, 8 H,  $\beta$ -pyrrole), 8.43 (d,  $J = 7.7$  Hz, 2H, Pyr-*H*), 8.35-8.30 (m, 8 H, Ar-*H* +  $\beta$ -pyrrole), 8.14 (AA'BB', d,  $J = 7.4$ , 4 H, Ar-*H*), 7.30 (s, 12 H, Ar-*H*), 2.65 (s, 18 H, Ar- $\text{CH}_3$ ), 1.88 (s, 36 H, Ar- $\text{CH}_3$ ).  $^{13}\text{C-NMR}$  (126 MHz,  $\text{CDCl}_3$ ):  $\delta$  150.23, 150.20, 150.04, 149.90, 143.69, 139.54, 139.29, 139.20, 137.69, 137.67, 134.87, 132.52, 132.15, 131.65, 131.48, 131.41, 131.08, 130.46, 130.18, 128.63, 127.91, 126.80, 125.63, 124.70, 122.74, 119.43, 119.26, 119.06, 118.92, 96.08, 89.78, 22.03, 21.96, 21.74. IR (KBr):  $\text{cm}^{-1}$  3446, 2921, 2851, 2337, 2030, 1952, 1639, 1432, 1384, 1112, 1061, 876, 616. MS (HR-

MALDI, DCTAB) found 1850.6505 (M+), C<sub>126</sub>H<sub>98</sub>N<sub>8</sub>Zn<sub>2</sub> requires 1850.6497.

**Zinc(II) 5,10,15-Trimesityl-20-(4-[2-(trimethylsilyl)ethynyl]phenyl)-porphyrin (2):** To a Schlenk tube, a solution of Zn(II)-5-(4-iodophenyl)-10,15,20,-trimesitylporphyrin<sup>[110]</sup> (50.0 mg, 53.7 μmol) in toluene/Et<sub>3</sub>N (5:1, 15.0 mL) was added and the whole was degassed with a freeze-pump-thaw cycle. After this, [Pd<sub>2</sub>(dba)<sub>3</sub>] (6.2 mg, 6.7 μmol) and AsPh<sub>3</sub> (8.2 mg, 26.7 μmol) were added and the suspension was subjected to another degassing cycle. Finally, TMSA (7.3 μL, 107.4 μmol) was added and all was degassed for the last time. All was stirred at room temperature overnight, under argon atmosphere. The reaction mixture was filtered over celite (with the aid of CH<sub>2</sub>Cl<sub>2</sub>), evaporated and purified by column chromatography (CHX/CH<sub>2</sub>Cl<sub>2</sub>, 85:15) to afford a dark purple solid which was further purified by precipitation from CH<sub>2</sub>Cl<sub>2</sub> with cold petroleum ether to obtain the pure product (83% yield, 41.0 mg). Characterizations were in accordance with literature.<sup>[110]</sup> m.p. > 300 °C. <sup>1</sup>H-NMR (500 MHz, CD<sub>2</sub>Cl<sub>2</sub>): δ 8.86 (d, J = 4.6 Hz, 2H, β-pyrrole), 8.76 (d, J = 4.6 Hz, 2H, β-pyrrole), 8.72 (s, 4 H, β-pyrrole), 8.20 (AA'BB', d, J = 7.6 Hz, 2H, Ar-H), 7.86 (AA'BB', d, J = 7.6 Hz, 2H, Ar-H), 7.31 (s, 6 H, Ar-H), 2.64 (s, 9 H, Ar-CH<sub>3</sub>), 1.85 (s, 6 H, Ar-CH<sub>3</sub>), 0.39 (s, 9 H, Si-CH<sub>3</sub>). <sup>13</sup>C-NMR (126 MHz, CD<sub>2</sub>Cl<sub>2</sub>): δ 151.83, 151.78, 151.64, 151.51, 145.26, 141.06, 141.02, 140.84, 140.79, 139.44, 136.27, 133.69, 132.97, 132.87, 132.49, 131.91, 129.57, 129.49, 124.09, 121.04, 120.80, 120.72, 106.98, 97.01, 23.31, 23.24, 23.05, 1.62. MS (HR-MS) found 899.3469 (M<sup>+</sup>), C<sub>58</sub>H<sub>54</sub>N<sub>4</sub>SiZn requires 898.3409.

**Modelling methodology.** When modelling compound **1**, all the coordination bonds between the Zn atoms and the porphyrins have been taken into account using harmonic restraints on the distances and angles between the Zn atoms and the nitrogen atoms of the porphyrins. When we built the [1·BPE]<sub>2</sub> complex, we added the necessary harmonic constraints to ensure all coordination bonds are considered and that the complex stays in the closed form geometry suggested by the experimental findings. When modelling the [1·BPE]<sub>2</sub> complex, the interactions between the molecules forming it and with the nanotubes are strong enough to overcome the restraints and deform the complex structure. To avoid such deformation, we explicitly introduce the solvent in the model, so that the complex is solvated and retains its actual structure. To do this, the complex is soaked and equilibrated into a periodic simulation box of chloroform, which was previously equilibrated at room temperature and pressure. In order to gain information on the way a single [1·BPE]<sub>2</sub> complex adsorbs on the nanotube, ideally, we should soak the nanotube and the complex in a solvent box large enough to contain both: this would hugely increase the computational time of the simulation due to the large number of solvent molecules required to fill such modelling box. To reduce the computational cost of the model, we consider that because of the use of a cut-off of 1.2 nm for the non-bonding interaction, most of the system will not contribute to the stability of the interface. Therefore, we replace the ideal model with the following system: the solvent box containing the solvated [1·BPE]<sub>2</sub> complex, has been placed in contact with a portion of the original nanotube wall having a

surface area of about 140 nm<sup>2</sup>. This slab of the nanotube wall is kept rigid during the simulations. Also, all the solvent molecules defining the edge of the solvent box have been frozen, to avoid their dispersion in the non-periodic modelling box. A few solvent molecules have been removed to reduce the liquid density and favour the diffusion.

## Acknowledgements

D.B. gratefully acknowledges the EU through the ERC Starting Grant "COLORLANDS" project, the MIUR through the FIRB ("SUPRACARBON", contract n° RBF10DAK6). Research in Mons is also supported by the FNRS-FRFC through the EOS program (2Dto3D project; contract O005018F) and the 'Consortium des Équipements de Calcul Intensif – CECI' program (grant number 2.5020.11). We thank Professor C. Hunter (University of Cambridge) for the help in trying to unravel the equilibria ruling the [1·(BPE)<sub>2</sub>] complex formation.

**Keywords:** Anisotropy • Carbon Nanotubes • Magnetic Field • Porphyrins • Supramolecular Chemistry

## References

- [1] S. Sengupta, F. Würthner, *Acc. Chem. Res.* **2013**, *46*, 2498–2512.
- [2] R. J. Cogdell, A. Gall, J. Köhler, *Q. Rev. Biophys.* **2006**, *39*, 227–324.
- [3] G. McDermott, S. M. Prince, A. A. Freer, A. M. Hawthornthwaite-Lawless, M. Z. Papiz, R. J. Cogdell, N. W. Isaacs, *Nature* **1995**, *374*, 517–521.
- [4] J.-M. Lehn, *Angew. Chem. Int. Ed.* **1990**, *29*, 1304–1319.
- [5] G. M. Whitesides, *Science* **2002**, *295*, 2418–2421.
- [6] D. N. Reinhoudt, *Science* **2002**, *295*, 2403–2407.
- [7] J. A. A. W. Elemans, A. E. Rowan, R. J. M. Nolte, *J. Mater. Chem.* **2003**, *13*, 2661–2670.
- [8] T. Aida, E. W. Meijer, S. I. Stupp, *Science* **2012**, *335*, 813–817.
- [9] S. I. Stupp, L. C. Palmer, *Chem. Mater.* **2014**, *26*, 507–518.
- [10] S. S. Babu, V. K. Praveen, A. Ajayaghosh, *Chem. Rev.* **2014**, *114*, 1973–2129.
- [11] X. Li, J. Yu, M. Jaroniec, *Chem. Soc. Rev.* **2016**, *45*, 2603–2636.
- [12] T. Mirkovic, E. E. Ostroumov, J. M. Anna, R. Van Grondelle, Govindjee, G. D. Scholes, *Chem. Rev.* **2017**, *117*, 249–293.
- [13] S. Kundu, A. Patra, *Chem. Rev.* **2017**, *117*, 712–757.
- [14] L.-L. Li, E. W.-G. Diau, *Chem. Soc. Rev.* **2013**, *42*, 291–304.
- [15] M. Urbani, M. Grätzel, M. K. Nazeeruddin, T. Torres, *Chem. Rev.* **2014**, *114*, 12330–12396.
- [16] A. Ajayaghosh, V. K. Praveen, *Acc. Chem. Res.* **2007**, *40*, 644–656.
- [17] E. Gomar-Nadal, J. Puigmartí-Luis, D. B. Amabilino, *Chem.*

- Soc. Rev. **2008**, *37*, 490–504.
- [18] L. Chen, D. W. McBranch, H.-L. Wang, R. Helgeson, F. Wudl, D. G. Whitten, *Proc. Natl. Acad. Sci. U. S. A.* **1999**, *96*, 12287–12292.
- [19] R. M. Jones, L. Lu, R. Helgeson, T. S. Bergstedt, D. W. McBranch, D. G. Whitten, *Proc. Natl. Acad. Sci. U. S. A.* **2001**, *98*, 14769–14772.
- [20] B.-K. An, S.-K. Kwon, S.-D. Jung, S. Y. Park, *J. Am. Chem. Soc.* **2002**, *124*, 14410–14415.
- [21] D. A. Heller, H. Jin, B. M. Martinez, D. Patel, B. M. Miller, T.-K. Yeung, P. V. Jena, C. Höbartner, T. Ha, S. K. Silverman, et al., *Nat. Nanotechnol.* **2009**, *4*, 114–120.
- [22] K. A. Mirica, J. G. Weis, J. M. Schnorr, B. Esser, T. M. Swager, *Angew. Chem. Int. Ed.* **2012**, *51*, 10740–10745.
- [23] M. Dionisio, J. M. Schnorr, V. K. Michaelis, R. G. Griffin, T. M. Swager, E. Dalcanale, *J. Am. Chem. Soc.* **2012**, *134*, 6540–6543.
- [24] J. Zhang, M. P. Landry, P. W. Barone, J.-H. Kim, S. Lin, Z. W. Ulissi, D. Lin, B. Mu, A. A. Boghossian, A. J. Hilmer, et al., *Nat. Nanotechnol.* **2013**, *8*, 959–968.
- [25] R. Pinalli, E. Dalcanale, F. Ugozzoli, C. Massera, *CrystEngComm* **2016**, *18*, 5788–5802.
- [26] C. Tudisco, M. E. Fragalà, A. E. Giuffrida, F. Bertani, R. Pinalli, E. Dalcanale, G. Compagnini, G. G. Condorelli, *J. Phys. Chem. C* **2016**, *120*, 12611–12617.
- [27] L. Maggini, D. Bonifazi, *Chem. Soc. Rev.* **2012**, *41*, 211–241.
- [28] M. L. Saha, S. De, S. Pramanik, M. Schmittel, *Chem. Soc. Rev.* **2013**, *42*, 6860–6909.
- [29] Q. Yan, Z. Luo, K. Cai, Y. Ma, D. Zhao, *Chem. Soc. Rev.* **2014**, *43*, 4199–4221.
- [30] A. Fihey, A. Perrier, W. R. Browne, D. Jacquemin, *Chem. Soc. Rev.* **2015**, *44*, 3719–3759.
- [31] P. Wei, X. Yan, F. Huang, *Chem. Soc. Rev.* **2015**, *44*, 815–832.
- [32] A. Corma, M. J. Díaz-Cabañas, J. L. Jordá, C. Martínez, M. Moliner, *Nature* **2006**, *443*, 842–845.
- [33] J. V. I. Timonen, M. Latikka, L. Leibler, R. H. A. Ras, O. Ikkala, *Science* **2013**, *341*, 253–257.
- [34] K. Keren, R. S. Berman, E. Buchstab, U. Sivan, E. Braun, *Science* **2003**, *302*, 1380–1382.
- [35] G. Accorsi, N. Armaroli, A. Parisini, M. Meneghetti, R. Marega, M. Prato, D. Bonifazi, *Adv. Funct. Mater.* **2007**, *17*, 2975–2982.
- [36] S. Srinivasan, S. S. Babu, V. K. Praveen, A. Ajayaghosh, *Angew. Chem. Int. Ed.* **2008**, *47*, 5746–5749.
- [37] F. Arcudi, V. Strauss, L. Đorđević, A. Cadranel, D. M. Guldi, M. Prato, *Angew. Chem. Int. Ed.* **2017**, *56*, 12097–12101.
- [38] J. A. Faiz, V. Heitz, J.-P. Sauvage, *Chem. Soc. Rev.* **2009**, *38*, 422–442.
- [39] F. D'Souza, O. Ito, *Chem. Commun.* **2009**, *0*, 4913–4928.
- [40] S. Mohnani, D. Bonifazi, *Coord. Chem. Rev.* **2010**, *254*, 2342–2362.
- [41] M. Jurow, A. E. Schuckman, J. D. Batteas, C. M. Drain, *Coord. Chem. Rev.* **2010**, *254*, 2297–2310.
- [42] M.-V. V. Martínez-Díaz, G. de la Torre, T. Torres, *Chem. Commun.* **2010**, *46*, 7090–7108.
- [43] M. Ethirajan, Y. Chen, P. Joshi, R. K. Pandey, *Chem. Soc. Rev.* **2011**, *40*, 340–362.
- [44] W. Auwärter, D. Ćcija, F. Klappenberger, J. V. Barth, *Nat. Chem.* **2015**, *7*, 105–120.
- [45] M. A. Rajora, J. W. H. Lou, G. Zheng, *Chem. Soc. Rev.* **2017**, *46*, 6433–6469.
- [46] I. Beletskaya, V. S. Tyurin, A. Y. A. Y. Tsivadze, R. Guillard, C. Stern, *Chem. Rev.* **2009**, *109*, 1659–1713.
- [47] S. S. Babu, D. Bonifazi, *ChemPlusChem* **2014**, *79*, 895–906.
- [48] L. Đorđević, N. Demitri, D. Bonifazi, *Supramol. Chem.* **2016**, *28*, 753–761.
- [49] L. Đorđević, T. Marangoni, F. De Leo, I. Papagiannouli, P. Aloukos, S. Couris, E. Pavoni, F. Monti, N. Armaroli, M. Prato, et al., *Phys. Chem. Chem. Phys.* **2016**, *18*, 11858–11868.
- [50] D. Milano, L. Đorđević, E. Zangrando, E. Iengo, P. Tecilla, *Inorganica Chim. Acta* **2016**, *453*, 376–384.
- [51] M. A. Rajora, J. W. H. Lou, G. Zheng, *Chem. Soc. Rev.* **2017**, *46*, 6433–6469.
- [52] A. Zieloniewska, F. Lodemeyer, A. Roth, D. M. Guldi, *Chem. Soc. Rev.* **2018**, *47*, 702–714.
- [53] A. Cadranel, V. Strauss, J. T. Margraf, K. A. Winterfeld, C. Vogl, L. Đorđević, F. Arcudi, H. Hoelzel, N. Jux, M. Prato, et al., *J. Am. Chem. Soc.* **2018**, *140*, 904–907.
- [54] K. M. Kadish, K. M. Smith, R. Guillard, *Handbook of Porphyrin Science*, World Scientific Publishing Company, **2010**.
- [55] M. O. Senge, *Chem. Commun.* **2011**, *47*, 1943–1960.
- [56] S. Hiroto, Y. Miyake, H. Shinokubo, *Chem. Rev.* **2017**, *117*, 2910–3043.
- [57] T. Sarma, P. K. Panda, *Chem. Rev.* **2017**, *117*, 2785–2838.
- [58] T. Chatterjee, V. S. Shetti, R. Sharma, M. Ravikanth, *Chem. Rev.* **2017**, *117*, 3254–3328.
- [59] M. Hoffmann, J. Kärnbratt, M.-H. Chang, L. M. Herz, B. Albinsson, H. L. Anderson, *Angew. Chem. Int. Ed.* **2008**, *47*, 4993–4996.
- [60] M. C. O'Sullivan, J. K. Sprafke, D. V. Kondratuk, C. Rinfray, T. D. W. Claridge, A. Saywell, M. O. Blunt, J. N. O'Shea, P. H. Beton, M. Malfois, et al., *Nature* **2011**, *469*, 72–75.
- [61] S. A. L. Rousseaux, J. Q. Gong, R. Haver, B. Odell, T. D. W. Claridge, L. M. Herz, H. L. Anderson, *J. Am. Chem. Soc.* **2015**, *137*, 12713–12718.
- [62] M. Rickhaus, A. Vargas Jentzsch, L. Tejerina, I. Grübner, M. Jirasek, T. D. W. Claridge, H. L. Anderson, *J. Am. Chem. Soc.* **2017**, *139*, 16502–16505.
- [63] P. S. Bols, H. L. Anderson, *Acc. Chem. Res.* **2018**, *51*, 2083–2092.
- [64] I.-W. Hwang, H. S. Cho, D. H. Jeong, D. Kim, A. Tsuda, T. Nakamura, A. Osuka, *J. Phys. Chem. B* **2003**, *107*, 9977–9988.

- [65] J.-S. S. Hu, Y.-G. G. Guo, H.-P. P. Liang, L.-J. Wan, L. Jiang, *J. Am. Chem. Soc.* **2005**, *127*, 17090–17095.
- [66] G. Bussetti, M. Campione, L. Ferraro, L. Raimondo, B. Bonanni, C. Goletti, M. Palumbo, C. Hogan, L. Duò, M. Finazzi, et al., *J. Phys. Chem. C* **2014**, *118*, 15649–15655.
- [67] S. Durot, J. Taesch, V. Heitz, *Chem. Rev.* **2014**, *114*, 8542–8578.
- [68] D. V. Kondratuk, J. K. Sprafke, M. C. O'Sullivan, L. M. A. Perdigo, A. Saywell, M. Malfois, J. N. O'Shea, P. H. Beton, A. L. Thompson, H. L. Anderson, *Chem. Eur. J.* **2014**, *20*, 12826–12834.
- [69] B. Zhu, H. Chen, W. Lin, Y. Ye, J. Wu, S. Li, *J. Am. Chem. Soc.* **2014**, *136*, 15126–15129.
- [70] P. Liu, Y. Hisamune, M. D. Peeks, B. Odell, J. Q. Gong, L. M. Herz, H. L. Anderson, *Angew. Chem. Int. Ed.* **2016**, *55*, 8358–8362.
- [71] L. Đorđević, F. Arcudi, A. D'Urso, M. Cacioppo, N. Micali, T. Bürgi, R. Purrello, M. Prato, *Nat. Commun.* **2018**, *9*, 3442.
- [72] A. D'Urso, M. E. Fragalà, R. Purrello, *Chem. Commun.* **2013**, *49*, 4441.
- [73] T. Tanaka, A. Osuka, *Chem. Soc. Rev.* **2015**, *44*, 943–969.
- [74] R. C. Haddon, A. Pasquarello, *Phys. Rev. B* **1994**, *50*, 16459–16463.
- [75] M. F. Lin, K. W. K. Shung, *Phys. Rev. B* **1995**, *52*, 8423–8438.
- [76] J. P. Lu, *Phys. Rev. Lett.* **1995**, *74*, 1123–1126.
- [77] A. Stopin, F. Pineux, R. Marega, D. Bonifazi, *Chem. Eur. J.* **2015**, *21*, 9288–9301.
- [78] A. Satake, Y. Miyajima, Y. Kobuke, *Chem. Mater.* **2005**, *17*, 716–724.
- [79] F. Cheng, S. Zhang, A. Adronov, L. Echegoyen, F. Diederich, *Chem. Eur. J.* **2006**, *12*, 6062–6070.
- [80] J. K. Sprafke, S. D. Stranks, J. H. Warner, R. J. Nicholas, H. L. Anderson, *Angew. Chem. Int. Ed.* **2011**, *50*, 2313–2316.
- [81] S. D. Stranks, J. K. Sprafke, H. L. Anderson, R. J. Nicholas, *ACS Nano* **2011**, *5*, 2307–2315.
- [82] C. Roquelet, F. Vialla, C. Diederichs, P. Roussignol, C. Delalande, E. Deleporte, J.-S. Lauret, C. Voisin, *ACS Nano* **2012**, *6*, 8796–8802.
- [83] F. Vialla, C. Roquelet, B. Langlois, G. G. Delpont, S. M. Santos, E. Deleporte, P. Roussignol, C. Delalande, C. Voisin, J.-S. S. Lauret, *Phys. Rev. Lett.* **2013**, *111*, 137402.
- [84] S. Srinivasan, V. K. Praveen, R. Philip, A. Ajayaghosh, *Angew. Chem. Int. Ed.* **2008**, *47*, 5750–5754.
- [85] P. Deria, C. D. Von Barga, J.-H. Olivier, A. S. Kumbhar, J. G. Saven, M. J. Therien, *J. Am. Chem. Soc.* **2013**, *135*, 16220–16234.
- [86] P. Deria, J.-H. Olivier, J. Park, M. J. Therien, *J. Am. Chem. Soc.* **2014**, *136*, 14193–14199.
- [87] R. Chamorro, L. De Juan-Fernández, B. Nieto-Ortega, M. J. Mayoral, S. Casado, L. Ruiz-González, E. M. Pérez, D. González-Rodríguez, *Chem. Sci.* **2018**, *9*, 4176–4184.
- [88] C. Romero-Nieto, R. García, M. Á. Herranz, C. Ehli, M. Ruppert, A. Hirsch, D. M. Guldi, N. Martín, *J. Am. Chem. Soc.* **2012**, *134*, 9183–9192.
- [89] F. G. Brunetti, C. Romero-Nieto, J. López-Andarias, C. Atienza, J. L. López, D. M. Guldi, N. Martín, *Angew. Chem. Int. Ed.* **2013**, *52*, 2180–2184.
- [90] C. Ehli, C. Oelsner, D. M. Guldi, A. Mateo-Alonso, M. Prato, C. Schmidt, C. Backes, F. Hauke, A. Hirsch, *Nat. Chem.* **2009**, *1*, 243–249.
- [91] C. Backes, F. Hauke, A. Hirsch, *Adv. Mater.* **2011**, *23*, 2588–2601.
- [92] T. Nakanishi, *Chem. Commun.* **2010**, *46*, 3425–3436.
- [93] Y. Shen, A. G. Skirtach, T. Seki, S. Yagai, H. Li, H. Möhwald, T. Nakanishi, *J. Am. Chem. Soc.* **2010**, *132*, 8566–8568.
- [94] Y. Shen, J. S. Reparaz, M. R. Wagner, A. Hoffmann, C. Thomsen, J.-O. Lee, S. Heeg, B. Hatting, S. Reich, A. Saeki, et al., *Chem. Sci.* **2011**, *2*, 2243–2250.
- [95] Y. Shen, T. Nakanishi, *Phys. Chem. Chem. Phys.* **2014**, *16*, 7199–7204.
- [96] K. S. Chichak, A. Star, M. V. P. Altoé, J. F. Stoddart, *Small* **2005**, *1*, 452–461.
- [97] M. S. Arnold, M. O. Guler, M. C. Hersam, S. I. Stupp, *Langmuir* **2005**, *21*, 4705–4709.
- [98] Y.-L. Zhao, J. F. Stoddart, *Acc. Chem. Res.* **2009**, *42*, 1161–1171.
- [99] A. Llanes-Pallas, K. Yoosaf, H. Traboulsi, J. Mohanraj, T. Seldrum, J. Dumont, A. Minoia, R. Lazzaroni, N. Armaroli, D. Bonifazi, *J. Am. Chem. Soc.* **2011**, *133*, 15412–15424.
- [100] L. Maggini, T. Marangoni, B. Georges, J. M. Malicka, K. Yoosaf, A. Minoia, R. Lazzaroni, N. Armaroli, D. Bonifazi, *Nanoscale* **2013**, *5*, 634–645.
- [101] T. Lei, X. Chen, G. Pitner, H.-S. P. Wong, Z. Bao, *J. Am. Chem. Soc.* **2016**, *138*, 802–805.
- [102] J. Lefebvre, J. Ding, Z. Li, P. Finnie, G. Lopinski, P. R. L. Malenfant, *Acc. Chem. Res.* **2017**, *50*, 2479–2486.
- [103] D. Fong, A. Adronov, *Chem. Sci.* **2017**, *8*, 7292–7305.
- [104] N. Nakashima, Y. Tomonari, H. Murakami, *Chem. Lett.* **2002**, *31*, 638–639.
- [105] D. M. Guldi, G. M. A. Rahman, N. Jux, D. Balbinot, N. Tagmatarchis, M. Prato, *Chem. Commun.* **2005**, *0*, 2038–2040.
- [106] A. de Juan, A. López-Moreno, J. Calbo, E. Ortí, E. M. Pérez, *Chem. Sci.* **2015**, *6*, 7008–7014.
- [107] E. M. Pérez, *Chem. Eur. J.* **2017**, *23*, 12681–12689.
- [108] D. P. Hickey, K. Lim, R. Cai, A. R. Patterson, M. Yuan, S. Sahin, S. Abdellaoui, S. D. Minter, *Chem. Sci.* **2018**, *9*, 5172–5177.
- [109] A. Pich, N. Schiemenz, V. Boyko, H.-J. P. Adler, *Polymer* **2006**, *47*, 553–560.
- [110] J. S. Lindsey, S. Prathapan, T. E. Johnson, R. W. Wagner, *Tetrahedron* **1994**, *50*, 8941–8968.
- [111] G. He, N. Yan, J. Yang, H. Wang, L. Ding, S. Yin, Y. Fang, *Macromolecules* **2011**, *44*, 4759–4766.
- [112] T. Kaposi, S. Joshi, T. Hoh, A. Wiengarten, K. Seufert, M.

- 
- Paszkiewicz, F. Klappenberger, D. Ćija, L. Đorđević, T. Marangoni, et al., *ACS Nano* **2016**, *10*, 7665–7674.
- [113] R. W. Wagner, T. E. Johnson, F. Li, J. S. Lindsey, *J. Org. Chem.* **1995**, *60*, 5266–5273.
- [114] E. Alessio, Ed., *Non-Covalent Multi-Porphyrin Assemblies*, Springer-Verlag, Berlin/Heidelberg, **2006**.
- [115] P. Thordarson, *Chem. Soc. Rev.* **2011**, *40*, 1305–1323.
- [116] A. Camara-Campos, C. A. Hunter, S. Tomas, *Proc. Natl. Acad. Sci. U. S. A.* **2006**, *103*, 3034–3038.
- [117] A. R. Mulholland, P. Thordarson, E. J. Mensforth, S. J. Langford, *Org. Biomol. Chem.* **2012**, *10*, 6045.
- [118] Y. Cohen, L. Avram, L. Frish, *Angew. Chem. Int. Ed.* **2005**, *44*, 520–554.
- [119] A. Macchioni, G. Ciancaleoni, C. Zuccaccia, D. Zuccaccia, *Chem. Soc. Rev.* **2008**, *37*, 479–489.
- [120] P. Timmerman, J.-L. Weidmann, K. A. Jolliffe, L. J. Prins, D. N. Reinhoudt, S. Shinkai, L. Frish, Y. Cohen, *J. Chem. Soc. Perkin Trans. 2* **2000**, 2077–2089.
- [121] A. I. Oliva, K. Gómez, G. González, P. Ballester, *New J. Chem.* **2008**, *32*, 2159.
- [122] L. Đorđević, T. Marangoni, T. Miletic, J. Rubio-Magnieto, J. Mohanraj, H. Amenitsch, D. Pasini, N. Liaros, S. Couris, N. Armaroli, et al., *J. Am. Chem. Soc.* **2015**, *137*, 8150–8160.
- [123] <http://accelrys.com/products/collaborative-science/biovia-materials-studio/>, “Accelrys Materials Studio 7,” can be found under <http://accelrys.com/products/collaborative-science/biovia-materials-studio/>, **2016**.
- [124] H. Sun, *J. Phys. Chem. B* **1998**, *102*, 7338–7364.
- [125] A. Minoia, Z. Guo, H. Xu, S. J. George, A. P. H. J. Schenning, S. De Feyter, R. Lazzaroni, *Chem. Commun.* **2011**, *47*, 10924–10926.
- [126] L. Maggini, M. Liu, Y. Ishida, D. Bonifazi, *Adv. Mater.* **2013**, *25*, 2462–2467.
- [127] I. O. Shklyarevskiy, P. Jonkheijm, P. C. M. Christianen, A. P. H. J. Schenning, A. Del Guerzo, J.-P. Desvergne, E. W. Meijer, J. C. Maan, *Langmuir* **2005**, *21*, 2108–2112.
- [128] M. Liebi, P. G. van Rhee, P. C. M. Christianen, J. Kohlbrecher, P. Fischer, P. Walde, E. J. Windhab, *Langmuir* **2013**, *29*, 3467–3473.
- [129] R. S. M. Rikken, R. J. M. Nolte, J. C. Maan, J. C. M. van Hest, D. A. Wilson, P. C. M. Christianen, *Soft Matter* **2014**, *10*, 1295–1308.
- [130] L. Wu, M. Ohtani, M. Takata, A. Saeki, S. Seki, Y. Ishida, T. Aida, *ACS Nano* **2014**, *8*, 4640–4649.
- [131] K. Sano, Y. Ishida, T. Aida, *Angew. Chem. Int. Ed.* **2018**, *57*, 2532–2543.
- [132] A. Stopin, A. Rossignon, M. Keshavarz, Y. Ishida, P. C. M. Christianen, D. Bonifazi, *Chem. Mater.* **2016**, *28*, 6985–6994.
- [133] I. Sanchez Esqueda, X. Yan, C. Rutherglen, A. Kane, T. Cain, P. Marsh, Q. Liu, K. Galatsis, H. Wang, C. Zhou, *ACS Nano* **2018**, *12*, 7352–7361.
- [134] I. Jeon, Y. Matsuo, S. Maruyama, *Top. Curr. Chem.* **2018**, *376*, 4.
- [135] V. Strauss, A. Roth, M. Sekita, D. M. Guldi, *Chem* **2016**, *1*, 531–556.
-

---

---